
The following resources related to this article are available online at <http://stke.sciencemag.org>.
This information is current as of 8 January 2014.

- Article Tools** Visit the online version of this article to access the personalization and article tools:
<http://stke.sciencemag.org/cgi/content/full/sigtrans;7/307/ra1>
- Supplemental Materials** "*Supplementary Materials*"
<http://stke.sciencemag.org/cgi/content/full/sigtrans;7/307/ra1/DC1>
- Related Content** The editors suggest related resources on *Science's* sites:
<http://stke.sciencemag.org/cgi/content/abstract/sigtrans;7/307/pe1>
<http://stke.sciencemag.org/cgi/content/abstract/sigtrans;6/304/ra104>
- References** This article has been **cited by** 1 article(s) hosted by HighWire Press; see:
<http://stke.sciencemag.org/cgi/content/full/sigtrans;7/307/ra1#BIBL>
- This article cites 54 articles, 23 of which can be accessed for free:
<http://stke.sciencemag.org/cgi/content/full/sigtrans;7/307/ra1#otherarticles>
- Glossary** Look up definitions for abbreviations and terms found in this article:
<http://stke.sciencemag.org/glossary/>
- Permissions** Obtain information about reproducing this article:
<http://www.sciencemag.org/about/permissions.dtl>

A Ligand-Independent VEGFR2 Signaling Pathway Limits Angiogenic Responses in Diabetes

Carmen M. Warren,¹ Safiyah Ziyad,¹ Anaïs Briot,¹ Aaron Der,¹ M. Luisa Iruela-Arispe^{1,2*}

Although vascular complications are a hallmark of diabetes, the molecular mechanisms that underlie endothelial dysfunction are unclear. We showed that reactive oxygen species generated from hyperglycemia promoted ligand-independent phosphorylation of vascular endothelial growth factor receptor 2 (VEGFR2). This VEGFR2 signaling occurred within the Golgi compartment and resulted in progressively decreased availability of VEGFR2 at the cell surface. Consequently, the responses of endothelial cells to exogenous VEGF in a mouse model of diabetes were impaired because of a specific deficiency of VEGFR2 at the cell surface, despite a lack of change in transcript abundance. Hyperglycemia-induced phosphorylation of VEGFR2 did not require intrinsic receptor kinase activity and was instead mediated by Src family kinases. The reduced cell surface abundance of VEGFR2 in diabetic mice was reversed by treatment with the antioxidant *N*-acetyl-L-cysteine, suggesting a causative role for oxidative stress. These findings uncover a mode of ligand-independent VEGFR2 signaling that can progressively lead to continuously muted responses to exogenous VEGF and limit angiogenic events.

INTRODUCTION

Diabetes is a prevalent metabolic disease and a growing health problem worldwide (1). Although diabetic conditions result in various pathologies, vascular complications account for most of the morbidity and mortality in diabetes, with cardiovascular disease causing up to 75% of deaths in diabetic patients (2). Diabetes leads to both macro- and microvascular problems characterized by endothelial dysfunction with severe consequences to wound healing (3, 4).

Increasing evidence suggests that oxidative stress, as a result of hyperglycemia, plays a key role in endothelial dysfunction (5). Several processes that promote injury are driven by hyperglycemia-induced overproduction of reactive oxygen species (ROS), including activation of protein kinase C (6) and the generation of advanced glycation end products (7), but can be prevented by overexpression of antioxidant enzymes (8).

ROS can activate many signaling components that modify endothelial function. At low concentrations, ROS act as signaling messengers that mediate cellular responses such as growth and migration. Hydrogen peroxide (H₂O₂) production is necessary for optimal receptor tyrosine kinase (RTK) signaling. Binding of growth factors to their receptors can stimulate a burst of ROS production, causing transient inhibition of phosphatases and increased kinase activity (9–11). However, the effects of sustained, long-term ROS on pathways that regulate normal endothelial cell function, as well as provide endothelial protection to damage, are less clear.

As a pivotal molecule in endothelial cell function, vascular endothelial growth factor (VEGF) regulates the formation, growth, and survival of blood vessels during physiological and pathological settings (12, 13). Deletion of a single allele of *Vegf* in mice results in early embryonic lethality due to lack of vascular development (14, 15). This underscores that regulation of VEGF signaling is sensitive to ligand abundance, and exquisite control is required at the transcriptional, translational, and posttranslational levels.

Proangiogenic signals initiated by VEGF are conveyed by the cell surface RTK VEGFR2 (VEGF receptor 2) (16). In the classical model of VEGFR2 activation, ligand binding results in dimerization and cross-phosphorylation

of two receptor monomers. Two residues in the cytoplasmic domain of VEGFR2, namely, Tyr¹⁰⁵⁴ and Tyr¹⁰⁵⁹, are required for autophosphorylation, and mutation of these amino acids completely blocks ligand-dependent phosphorylation (17).

Inhibition of the VEGF-VEGFR2 signaling axis has been correlated with the state of endothelial dysfunction typical of diabetes (18, 19). However, it is largely unknown how VEGF signaling is affected at the molecular level in diabetes. In our study, we evaluated VEGFR2 signaling under high-glucose conditions using both in vivo and in vitro models. Combined, the findings uncovered that high-glucose exposure induces ligand- and intrinsic kinase-independent VEGFR2 phosphorylation in the Golgi that impairs trafficking of receptors to the cell surface. The outcome is a progressive reduction in VEGFR2 at the plasma membrane, muting angiogenic responses in diabetes.

RESULTS

Endothelial cells of diabetic mice are less responsive to VEGF in vivo

To understand the role of VEGF signaling in the compromised endothelium during diabetes, we evaluated angiogenic responses in mice homozygous for the obese spontaneous mutation (*ob/ob*), which develop hyperglycemia at about 4 weeks of age (fig. S1A) (20). Consistent with previous reports, *ob/ob* diabetic mice displayed impaired vascular growth in wound healing and in matrix angiogenesis assays (Fig. 1, A to E) (21). This deficiency occurred despite similar *Vegfr2* (fig. S1B) and increased *Vegfa* transcript abundance (fig. S1C) in the wounded skin of *ob/ob* mice.

We also examined the ability of VEGF to activate VEGFR2 in vivo to further investigate the underlying mechanisms for the differences observed. A brief lung perfusion of *ob/ob* mice with VEGF revealed a 2.5-fold reduction in the phosphorylation of VEGFR2 compared to wild-type littermate controls (Fig. 1, F and G). Moreover, although transcript abundance was similar, total VEGFR2 protein was twofold lower in *ob/ob* mice than in wild-type mice (Fig. 1, H and I). *Vegfa* mRNA was not significantly different in the lungs of *ob/ob* mice (fig. S1D). These findings implied that post-translational events were involved in the decreased abundance of VEGFR2 because total protein, but not mRNA, differed.

¹Department of Molecular, Cell and Developmental Biology, University of California, Los Angeles, Los Angeles, CA 90095, USA. ²Molecular Biology Institute, University of California, Los Angeles, Los Angeles, CA 90095, USA.

*Corresponding author. E-mail: arispe@mcdm.ucla.edu

To determine whether the effects on VEGFR2 in the endothelium of *ob/ob* mice were due to hyperglycemia, rather than associated with complications from obesity, we used a second diabetic model. VEGFR2 phosphorylation and total receptor abundance were evaluated in streptozotocin (STZ)-induced diabetic mice (fig. S1E). Similar to *ob/ob* mice, STZ mice also showed a greater than two-fold decrease in VEGFR2 phosphorylation (Fig. 1, J and K) upon perfusion with VEGF. In addition, STZ mice showed 40% less VEGFR2 at the protein level (Fig. 1L), but did not exhibit statistically significant changes in *Vegfr2* or *Vegfa* transcripts when compared to control (Fig. 1M and fig. S1F).

Exposure of endothelial cells to high glucose impairs migration and VEGFR2 activation

To assess the effects of hyperglycemia on VEGFR2 *in vitro*, we grew human umbilical vein endothelial cells (HUVECs) under normal glucose (5 mM) or high-glucose (25 mM) conditions. Consistent with the results obtained from diabetic mice, exposure to high glucose for 5 days reduced the ability of HUVECs to respond to VEGF by fourfold (Fig. 2, A and B). To determine the impact of these changes on endothelial cell function, we performed a wound closure migration assay. HUVECs cultured in the presence of high glucose migrated at a slower rate than cells cultured with normal glucose concentrations, under both basal conditions and in response to VEGF (Fig. 2, C and D, and fig. S2, A and B).

Although endothelial cells exposed to high glucose were functionally impaired in their response to VEGF, total VEGFR2 protein was not significantly altered (Fig. 2E). This was in contrast to the long-term diabetic mouse models. We hypothesized that the reduced response to VEGF was due to decreased VEGFR2 availability at the cell surface. Indeed, cell surface biotinylation assays revealed a marked decrease in the surface abundance of VEGFR2 in HUVECs exposed to high glucose (Fig. 2, F and G). Furthermore, fractionation of HUVECs into membrane, Golgi, and other vesicular pools confirmed reduced VEGFR2 at the cell membrane upon high-glucose exposure (Fig. 2, H and I). Additionally, Scatchard analysis of VEGF-E, a ligand specific to VEGFR2, revealed a decrease in the number of ligand-binding sites in HUVECs cultured under 25 mM glucose (0.54×10^4 per cell) compared to 5 mM glucose (3.5×10^4 per cell) (Fig. 2J). Similar results were obtained for

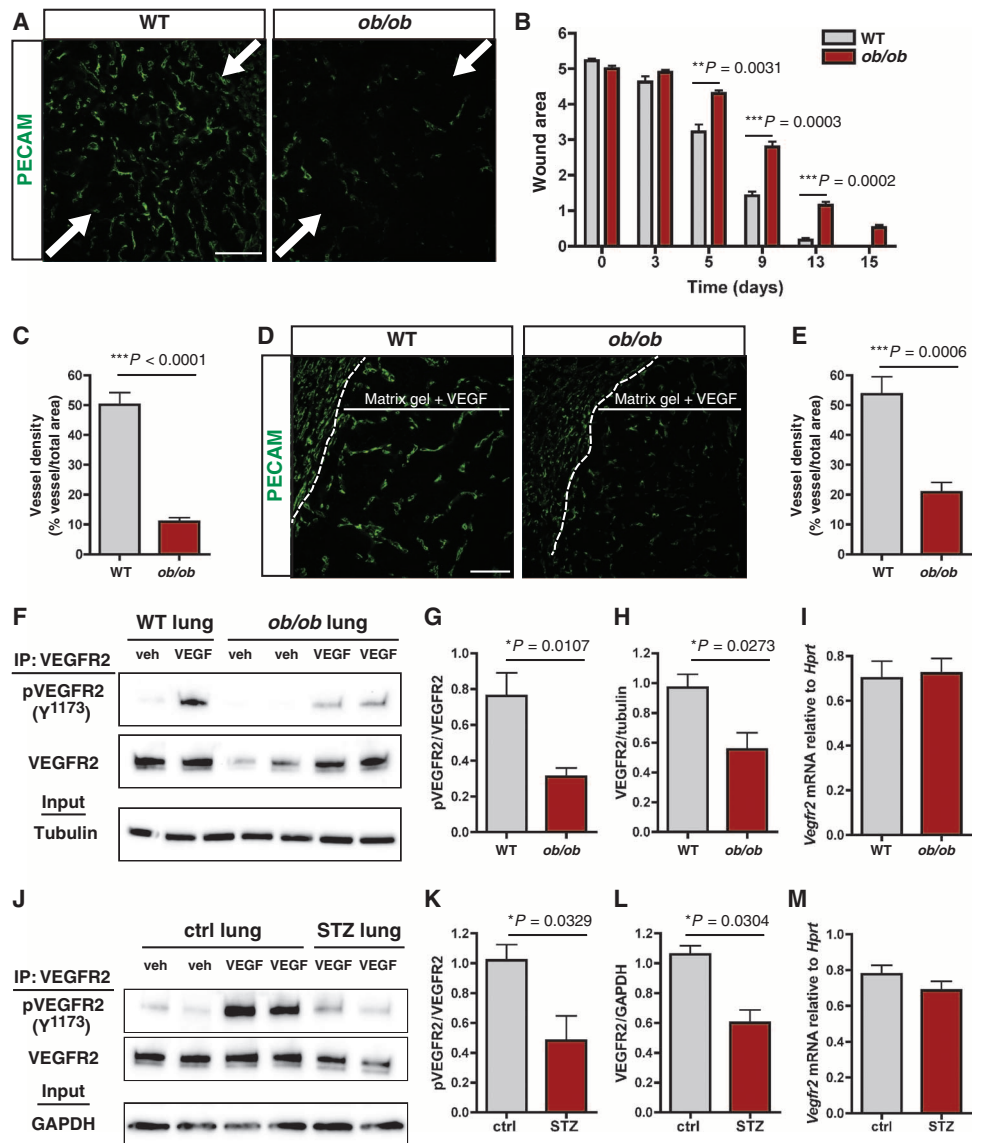


Fig. 1. Endothelial cells of diabetic mice are less responsive to VEGF *in vivo*. (A) Immunofluorescence of vessels [platelet endothelial cell adhesion molecule (PECAM), green] 15 days after wounding. Arrows point to wound area. WT, wild type. Scale bar, 50 μ m. (B) Quantification of wound area; $n = 4$ mice. (C) Quantification of vessel density; $n = 7$ mice. (D) Immunofluorescence of vessels (PECAM, green) 7 days after matrix gel implant. Scale bar, 50 μ m. (E) Quantification of vessel density; $n = 6$ mice. (F) Immunoblot of phosphorylated (p) and total VEGFR2 after perfusion with VEGF or vehicle (veh), after immunoprecipitation of VEGFR2 from lungs of *ob/ob* and WT mice. Tubulin immunoblot of input is shown. (G) Quantification of pVEGFR2/total VEGFR2 from lungs of WT and *ob/ob* mice; $n = 6$ mice. (H) Quantification of total VEGFR2/tubulin from lungs of WT and *ob/ob* mice; $n = 4$ mice. (I) Quantitative reverse transcription polymerase chain reaction (RT-PCR) of *Vegfr2* in lungs from WT and *ob/ob* mice, relative to *Hprt*; $n = 10$ mice. (J) Immunoblot of total VEGFR2 and pVEGFR2 after perfusion with VEGF or vehicle, and immunoprecipitation of VEGFR2 from lungs of STZ or control (ctrl) mice. Glyceraldehyde-3-phosphate dehydrogenase (GAPDH) immunoblot of input. (K) Quantification of pVEGFR2/total VEGFR2 from lungs of control and STZ animals; $n = 4$ mice. (L) Quantification of total VEGFR2/GAPDH from lungs of control and STZ animals; $n = 3$ mice. (M) Quantitative RT-PCR of *Vegfr2* in lungs of control and STZ mice, relative to *Hprt*; $n = 6$ mice. Data represent means \pm SEM and were analyzed using a Student's *t* test.

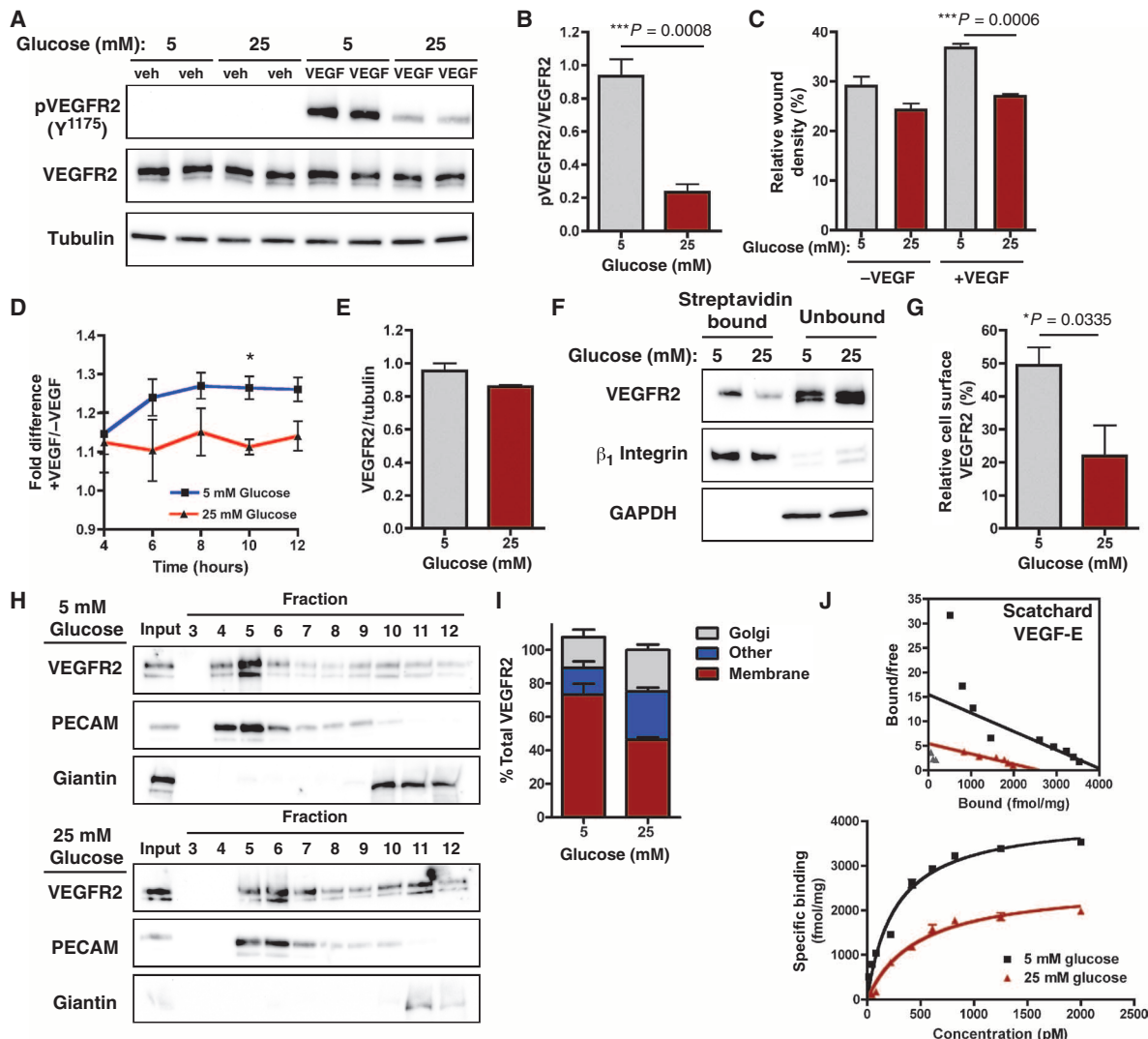


Fig. 2. Hyperglycemia impairs responses of endothelial cells to VEGF in vitro. (A and B) HUVECs cultured under 5 or 25 mM glucose were exposed to VEGF. Immunoblot of total VEGFR2, pVEGFR2, and tubulin (A). Quantification of pVEGFR2/total VEGFR2 (B). *n* = 3 to 4 sets of cells. (C) Wound closure migration assay of HUVECs grown under 5 or 25 mM glucose ± VEGF. Relative wound density was plotted 10 hours after wounding. *n* = 3 sets of cells. (D) Wound closure migration plotted as fold difference of relative wound density in response to VEGF compared to untreated cells. *n* = 3 sets of cells, **P* = 0.0126. (E) Quantification of VEGFR2/tubulin from HUVECs grown in 5 or 25 mM glucose. *n* = 3 to 4 sets of cells. (F) Immu-

noblot of HUVECs grown under 5 or 25 mM glucose and subjected to cell surface biotinylation assays. Streptavidin bound represents the cell surface fraction, and unbound represents intracellular pool. β_1 Integrin and GAPDH are the cell surface and intracellular controls, respectively. (G) Quantification of relative streptavidin-bound (cell surface) VEGFR2. *n* = 3 sets of cells. (H) Immunoblot of VEGFR2 after cell fractionation of HUVECs grown under 5 or 25 mM glucose. (I) Quantification of VEGFR2 in cell fractions as % of total VEGFR2. *n* = 3 sets of cells. (J) Scatchard plot analysis of VEGF-E binding to HUVECs grown in 5 or 25 mM glucose. *n* = 3 sets of cells. Data represent means ± SEM and were analyzed using a Student's *t* test.

VEGF-A (fig. S2C). These findings explained the decreased extent of VEGF-induced phosphorylation of VEGFR2 and the reduced migratory responses to the growth factor.

Hyperglycemia results in the production of ROS, which induces VEGFR2 phosphorylation and degradation

Several lines of evidence suggest that the effect of hyperglycemia on endothelial dysfunction is due to an increase in oxidative stress (5). HUVECs cultured under high glucose exhibited increased ROS production, as detected by fluorescence of dichlorodihydrofluorescein (DCF), compa-

able to direct treatment with glucose oxidase (GO), which catalyzes the oxidation of glucose into H₂O₂ (Fig. 3, A and B). Consistent with hyperglycemia in vivo, VEGFR2 abundance was also reduced by ROS in a time-dependent manner in vitro (Fig. 3, C to G). In addition, treatment with either GO or H₂O₂ resulted in marked phosphorylation of VEGFR2 in HUVECs and other endothelial cell types (Fig. 3, C, D, and H, and fig. S3, A to C). ROS-induced phosphorylation, especially in the presence of GO, was considerably greater than phosphorylation achieved by VEGF stimulation (Fig. 3, C, D, and H) and coincided with a decrease in VEGFR2 abundance (Fig. 3, C to H).

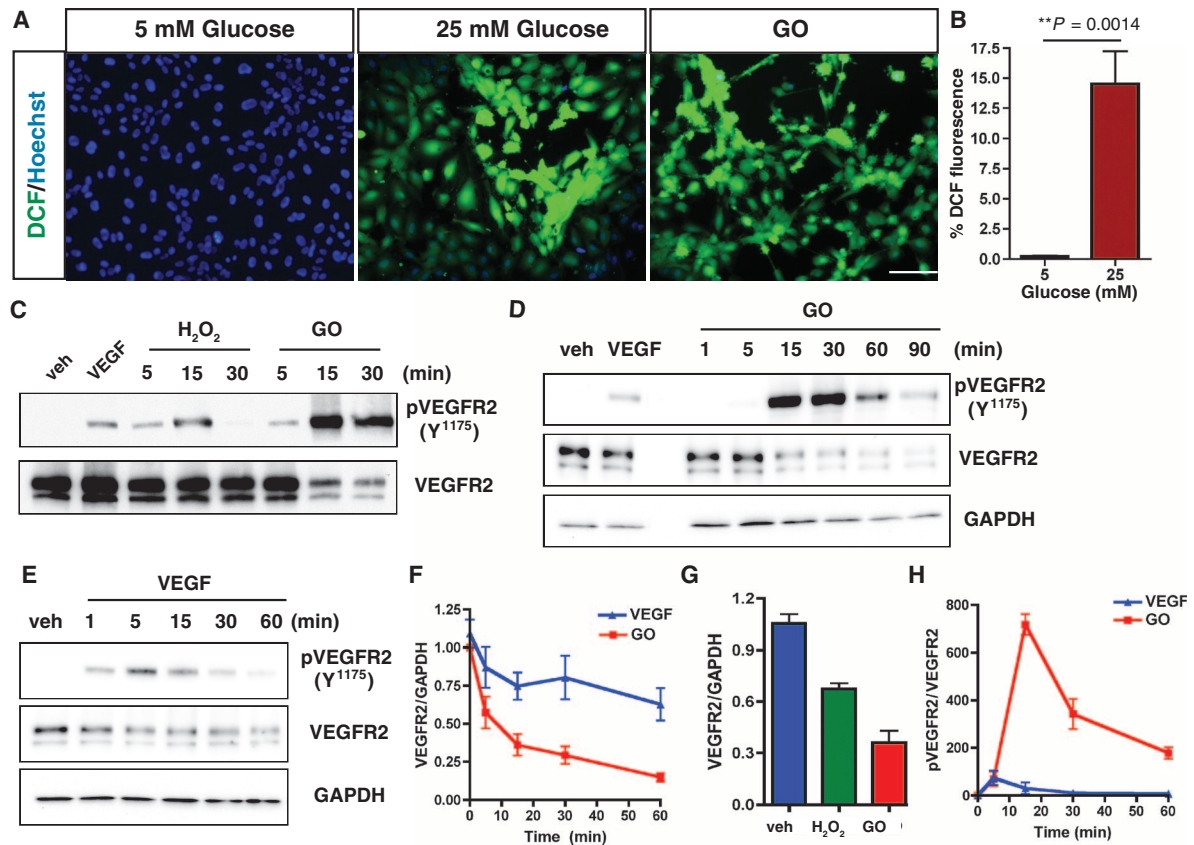


Fig. 3. High glucose generates ROS production, which induces VEGFR2 phosphorylation and degradation. (A) HUVECs grown in 5 or 25 mM glucose or treated with GO as indicated were imaged with the ROS indicator DCF (green) and Hoechst 33342 (blue) as a nuclear counterstain. Scale bar, 50 μ m. (B) Quantification of relative DCF fluorescence. $n = 15$ to 25 images from three sets of cells. (C to E) Immunoblot of total VEGFR2 and pVEGFR2

from HUVECs treated with H₂O₂ (C), GO (C and D), or VEGF (C to E) for the indicated times. (F) Kinetics of VEGFR2/GAPDH in HUVECs treated with VEGF or GO. $n = 3$ sets of cells. (G) Quantification of VEGFR2/GAPDH from HUVECs treated with H₂O₂ or GO. $n = 3$ sets of cells. (H) Kinetics of pVEGFR2/total VEGFR2 in HUVECs treated with VEGF or GO. $n = 3$ sets of cells. Data represent means \pm SEM and were analyzed using a Student's t test.

ROS-induced VEGFR2 phosphorylation is ligand- and VEGFR2 kinase-independent and requires Src kinases

To further dissect the mechanism of ROS-induced phosphorylation of VEGFR2, we asked whether these phosphorylation events were triggered by endothelial cell-derived VEGF (22). Treatment of cells with anti-VEGF antibodies, which prevent VEGF from binding to its receptors, did not block H₂O₂-mediated phosphorylation of VEGFR2 (Fig. 4A). Although neutralizing antibodies can inactivate secreted VEGF, they are unable to block intracellular pools of the ligand. Therefore, we compared the response of cultured endothelial cells derived from wild-type mice and mice with an endothelial cell-specific knockout of VEGF to ROS treatment. Wild-type and VEGF-null endothelial cells showed comparable responses to H₂O₂, suggesting that ligand was dispensable for ROS-induced VEGFR2 phosphorylation (Fig. 4B).

We next asked whether the intrinsic kinase activity of VEGFR2 was required for ROS-induced VEGFR2 phosphorylation. Treatment with the VEGFR kinase inhibitor SU4312 completely impaired VEGF-mediated activation of VEGFR2 but did not block phosphorylation of the receptor upon exposure to ROS (Fig. 4C). The findings implied that VEGFR2 was activated through a mechanism other than transphosphorylation.

Similar to other RTKs, the cytoplasmic domain of VEGFR2 contains several tyrosine residues that, when phosphorylated, act as docking sites

for second messengers. There are also two tyrosines (Tyr¹⁰⁵⁴ and Tyr¹⁰⁵⁹) that function as kinase regulatory residues and must be phosphorylated for activation of the kinase domain (Fig. 4D). Accordingly, we evaluated the status of the tyrosine residues in VEGFR2 that become phosphorylated as a consequence of ligand binding. Although the pattern of tyrosine phosphorylation upon treatment with VEGF was similar to previous reports, the kinase regulatory tyrosine residues Tyr¹⁰⁵⁴ and Tyr¹⁰⁵⁹ were not phosphorylated upon ROS exposure (either GO or H₂O₂) (Fig. 4E). These findings were further confirmed by expression of a kinase-dead VEGFR2 construct (Y1054F/Y1059F) in 293 cells (Fig. 4F). Kinase-dead VEGFR2 was not phosphorylated in the presence of VEGF, but was still phosphorylated upon ROS treatment. Furthermore, complete deletion of the extracellular domain of VEGFR2 did not impair ROS-mediated VEGFR2 phosphorylation (Fig. 4F). Together, our data indicate that ROS-induced phosphorylation is both ligand-independent and VEGFR2 kinase-independent.

Activation of another member of the VEGFR family, VEGFR3, can occur in a ligand-independent manner and through the activity of Src (23, 24). Therefore, we examined whether Src kinases were required for VEGFR2 phosphorylation upon ROS exposure. Treatment with H₂O₂ resulted in phosphorylation of Src with kinetics similar to that of VEGFR2 (fig. S4A). The Src kinase family inhibitor PP2 did not affect VEGF-induced VEGFR2

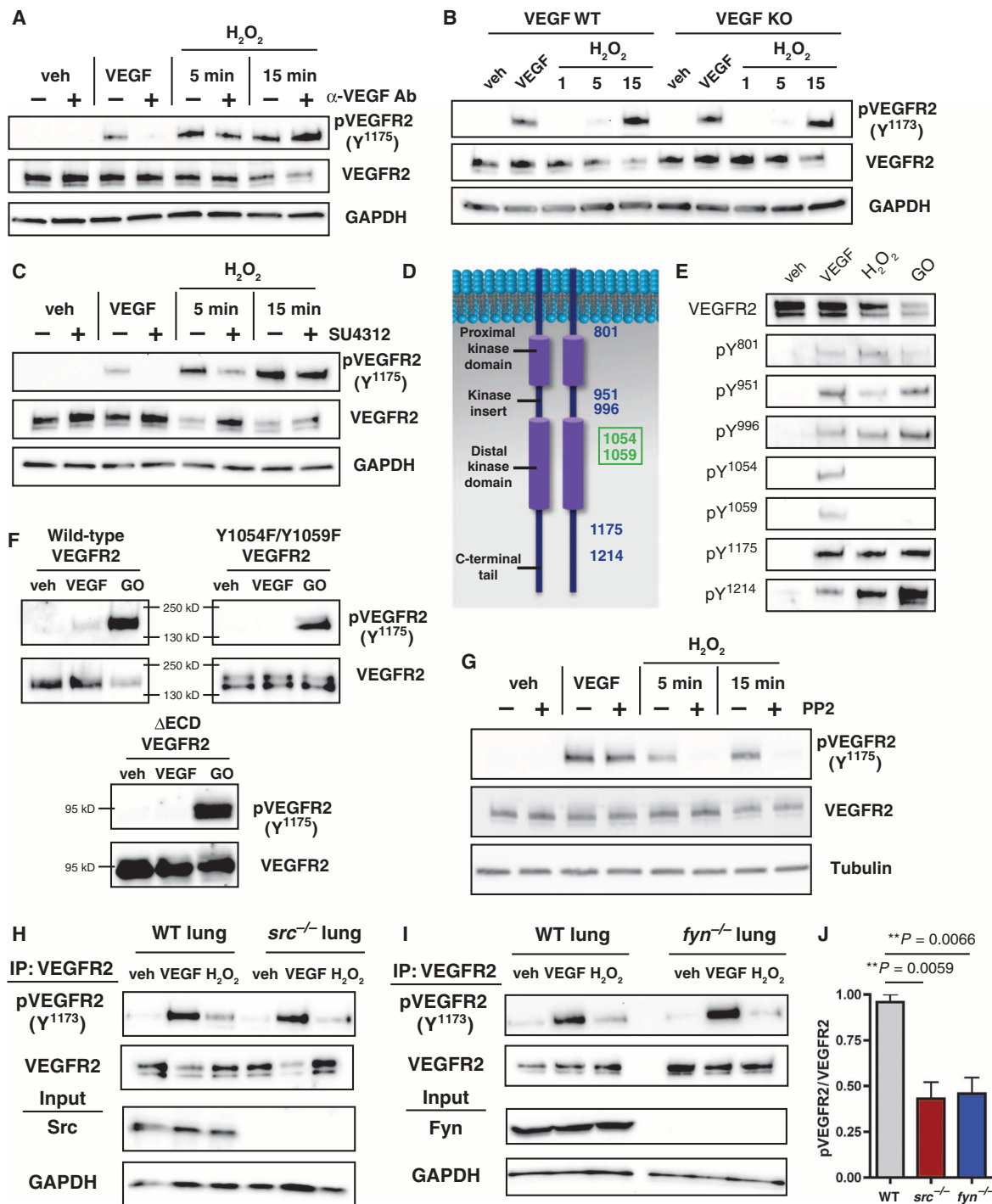


Fig. 4. ROS-induced VEGFR2 phosphorylation is ligand- and intrinsic kinase-independent and mediated by Src family kinases. (A) Immunoblot of total VEGFR2 and pVEGFR2 in HUVECs treated with VEGF or H₂O₂, ± anti-VEGF antibody. *n* = 3 sets of cells. (B) Immunoblot analysis of total VEGFR2 and pVEGFR2 in VEGF-null and WT mouse liver endothelial cells treated with VEGF or H₂O₂. *n* = 4 sets of cells. (C) Immunoblot of total VEGFR2 and pVEGFR2 in HUVECs treated with VEGF or H₂O₂, ± SU4312. *n* = 3 sets of cells. (D) Schema of the tyrosine residues in the VEGFR2 cytoplasmic domain. (E) Immunoblot of each phosphotyrosine in the VEGFR2 tail after immunoprecipitation of

VEGFR2 in HUVECs treated with VEGF, H₂O₂, or GO. (F) Immunoblot of total VEGFR2 and pVEGFR2 in 293 cells expressing WT, kinase-dead (Y1054F/Y1059F), or extracellular domain-deleted (ΔECD) VEGFR2. *n* = 2 sets of cells. (G) Immunoblot of total VEGFR2 and pVEGFR2 in HUVECs treated with VEGF or H₂O₂ ± PP2. *n* = 3 sets of cells. (H and I) Immunoblot of total VEGFR2 and pVEGFR2 in lungs from WT, *src*^{-/-} (H), or *fyn*^{-/-} (I) mice perfused with VEGF or H₂O₂. (J) Quantification of H₂O₂-mediated changes in the pVEGFR2/total VEGFR2 ratio is shown relative to WT mice. *n* = 3 mice. Data represent means ± SEM and were analyzed using a Student's *t* test.

phosphorylation, but did prevent H₂O₂-mediated phosphorylation of VEGFR2 (Fig. 4G). Furthermore, ROS-induced VEGFR2 phosphorylation was decreased twofold in the lungs of Src or Fyn knockout mice perfused with H₂O₂ compared to those of wild-type controls (Fig. 4, H to J). In addition, small interfering RNA (siRNA)-mediated knockdown of Src, Fyn, or Yes blocked ROS-induced VEGFR2 phosphorylation by roughly twofold (fig. S4B). Inhibition of Src kinases by PP2 blocked activation of Tyr⁹⁵¹ and Tyr¹¹⁷⁵ more effectively than the other residues (fig. S4C). These results suggest that Src family kinases can mediate ROS-induced VEGFR2 phosphorylation, although there appears to be redundancy and compensation between members.

An open question was whether other RTKs behave in a similar manner. We found that Tie2, another RTK found on endothelial cells, is also activated by ROS through Src (fig. S5, A to D), although this activation does not result in reduction of Tie2 protein as it does with VEGFR2 (fig. S5B).

Finally, we examined whether ROS-mediated phosphorylation of VEGFR2 resulted in downstream signaling. Phospholipase C- γ (PLC- γ) and p38 are targets of VEGFR2 (25); however, PLC- γ , but not p38, was phosphorylated by Src-mediated ligand-independent VEGFR2 signaling (fig. S5E). The findings indicate that ligand and ligand-independent activation of VEGFR2 are likely to yield distinct signaling outcomes.

ROS-induced VEGFR2 phosphorylation occurs in the Golgi

Next, to uncover how ROS-induced VEGFR2 phosphorylation affected VEGFR2 abundance and localization, we performed immunofluorescence for total and phosphorylated VEGFR2. ROS stimulation led to substantial phosphorylation of VEGFR2 located in the Golgi (Fig. 5, A to D). In addition, the Golgi pool of VEGFR2 was reduced upon ROS treatment (Fig. 5, A and C). Furthermore, a fraction of activated Src was localized in the Golgi upon ROS treatment (fig. S6, A and B), consistent with our results implicating Src as an upstream activator of VEGFR2.

To confirm that phosphorylation of VEGFR2 in response to ROS was predominantly intracellular, rather than at the cell surface, we performed cell surface proteolysis assays. As expected, shedding of cell surface VEGFR2 before VEGF stimulation blocked VEGFR2 activation. In contrast, cells subjected to external proteolysis still exhibited VEGFR2 phosphorylation when exposed to ROS (Fig. 5E).

We then determined the abundance of VEGFR2 at the plasma membrane and within intracellular stores after ROS treatment using cell surface biotinylation assays. Upon GO stimulation, intracellular VEGFR2 was substantially reduced, whereas cell surface VEGFR2 was largely unaffected (Fig. 5, F and G). As previously reported (26), we also noted that stimulation with VEGF promoted a transient increase or stabilization of cell surface VEGFR2 protein abundance (Fig. 5F). Because activation of VEGFR2 results in receptor degradation (27), the reduction in intracellular VEGFR2 protein abundance is consistent with a burst of VEGFR2 phosphorylation in the Golgi compartment, and not at the cell surface.

Subsequently, we sought to reconcile results from initial experiments (Fig. 2, F and J) indicating that chronic hyperglycemia leads to reduction of cell surface VEGFR2, whereas a burst of ROS leads to decreased abundance of an intracellular, Golgi-localized pool of VEGFR2. In this regard, it is important to recall that disruption of endosomal trafficking from the Golgi to the plasma membrane initially triggers degradation of the Golgi pool of VEGFR2, which eventually results in decreased cell surface VEGFR2 (28). We predicted that hyperglycemia and ROS might yield a similar outcome, whereby acute exposure to ROS is unlikely to alter cell surface abundance of VEGFR2; however, in a chronic situation, a concurrent reduction in plasma membrane-localized VEGFR2 is likely to occur. To test this hy-

pothesis, we performed pulse-chase experiments in which VEGFR2 abundance was monitored in HUVECs subjected to an acute burst of ROS. Similar cultures received a short treatment with extracellular VEGF, which results in a transient reduction of cell surface VEGFR2. We also used a combination of VEGF and GO stimulation to deplete both plasma membrane and Golgi pools and predicted an enhanced effect. Indeed, with acute ROS stimulation and a recovery time of 12 hours, we observed that the cell surface pool of VEGFR2 was reduced (Fig. 5, H and I) and that HUVECs were less responsive to VEGF, using phosphorylated VEGFR2 as a readout (Fig. 5, J and K).

Antioxidants rescue the effects of ROS on endothelial cells

To further test whether the effects observed on endothelial cells under hyperglycemic conditions were in fact due to ROS production, we performed experiments in the presence of the antioxidant *N*-acetyl-L-cysteine (NAC) (9, 29). NAC effectively blocked ROS production in endothelial cultures as a result of H₂O₂ and GO treatment (Fig. 6, A and B). NAC also decreased VEGFR2 phosphorylation in response to H₂O₂ (ligand-independent signaling), whereas it had no effect on VEGF-mediated phosphorylation of VEGFR2 (ligand-dependent activation) (Fig. 6C). Furthermore, in cell surface biotinylation assays, NAC treatment under high-glucose conditions rescued the abundance of cell surface VEGFR2 similar to that observed under normal glucose (Fig. 6, D and E). Moreover, cells cultured under high glucose and exposed to NAC showed increased response to VEGF stimulation, as indicated by phosphorylation of VEGFR2 (Fig. 6, F and G), compared to cells treated with high glucose alone. In addition, NAC rescued the functional defects observed in endothelial cells under high-glucose conditions. In wound closure migration assays, cells cultured with NAC and in the presence of high glucose migrated faster than cells grown in high glucose alone, and to a similar rate as cells grown under normal glucose (Fig. 6H).

The experiments in vitro supported the conclusion that hyperglycemia-generated ROS promoted ligand-independent VEGFR2 signaling. Furthermore, under long-term exposure to glucose, this phosphorylation resulted in extensive use of VEGFR2 in the Golgi, depleting intracellular stores and subsequently affecting cell surface abundance of VEGFR2. To confirm these results in vivo, we assessed cell surface and intracellular pools of VEGFR2 protein in *ob/ob* and wild-type mice, using an in vivo cell surface biotinylation assay. In addition to the significant decrease in total protein abundance (Fig. 1H), we found that the ratio of cell surface to total VEGFR2 was also affected in *ob/ob* mice, despite equivalent biotinylation of the endothelial cell surface as shown by biotin immunofluorescence (Fig. 7, A and B). *ob/ob* mice showed a 40% reduction in the cell surface abundance of VEGFR2, as well as a significant decrease in intracellular VEGFR2 (Fig. 7C). Subsequently, we evaluated the abundance of VEGFR2 at progressive ages, ranging from 2 to 6 months. The findings demonstrated that the cell surface abundance of VEGFR2 protein was progressively reduced in older *ob/ob* mice (Fig. 7, D and E). This effect was not detected for other cell surface proteins (β_1 integrin and PECAM).

Finally, we treated *ob/ob* mice with the antioxidant NAC to determine whether the effects of hyperglycemia on VEGFR2 phosphorylation in response to VEGF could be rescued. Although *ob/ob* mice exposed to constant NAC remained hyperglycemic, phosphorylation of VEGFR2 in response to VEGF was comparable to that in wild-type mice (Fig. 7, F and G).

DISCUSSION

Although vascular complications have long been associated with diabetes, the complex series of events that lead to endothelial dysfunction in a hyperglycemic setting are less understood. Here, we showed that high-glucose

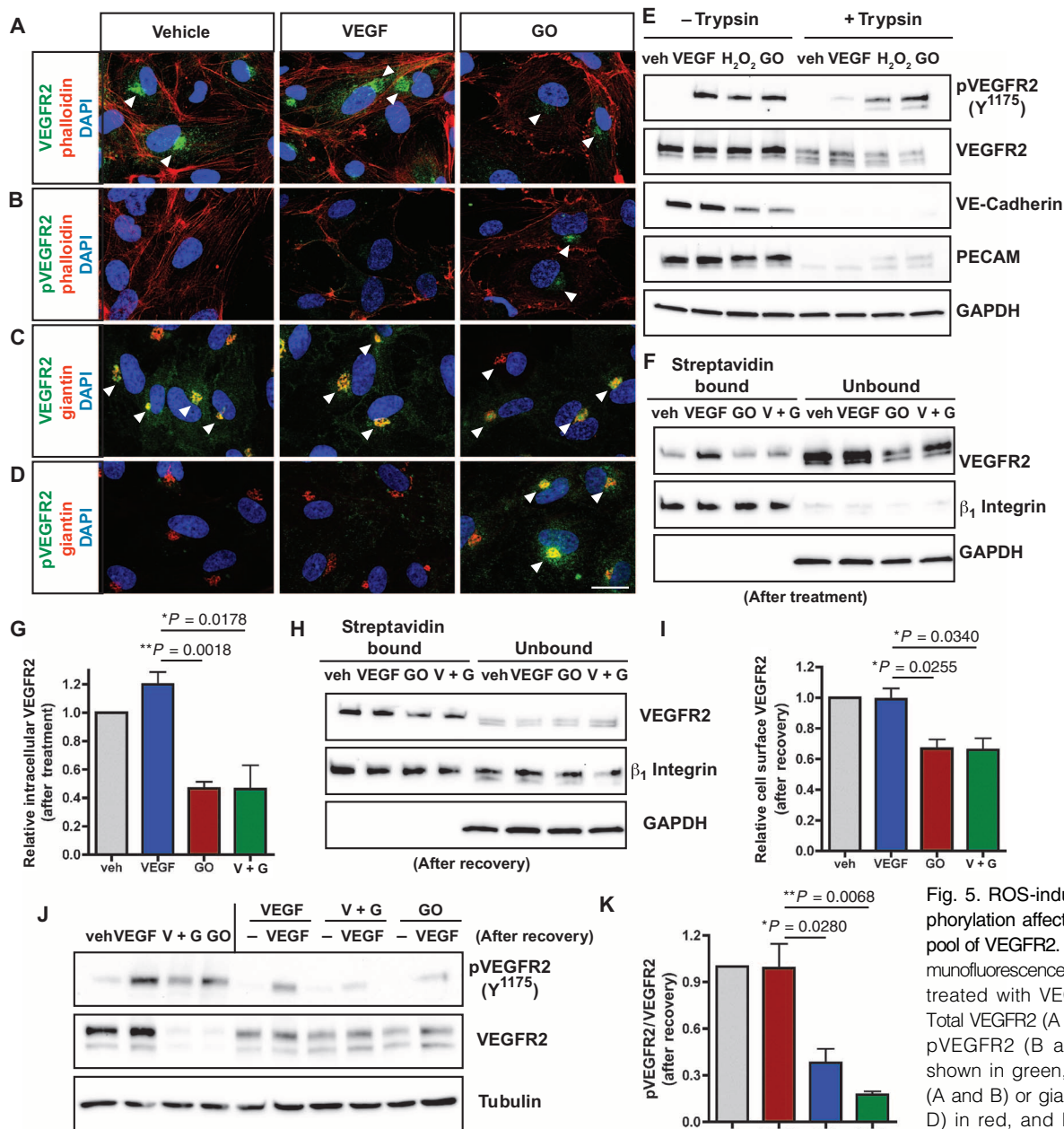


Fig. 5. ROS-induced phosphorylation affects the Golgi pool of VEGFR2. (A to D) Immunofluorescence of HUVECs treated with VEGF or GO. Total VEGFR2 (A and C) and pVEGFR2 (B and D) are shown in green, phalloidin (A and B) or giantin (C and D) in red, and DAPI (4',6-diamidino-2-phenylindole) in blue. Scale bar, 20 μm. *n* = 3 sets of cells. (E) Immunoblot of total VEGFR2 and pVEGFR2 in HUVECs exposed to trypsin and then VEGF, H₂O₂, or GO. VE (vascular endothelial)-cadherin and PECAM are shown as membrane controls and GAPDH as an intracellular control. *n* = 3 sets of cells. (F and G) Cell surface biotinylation to separate membrane (streptavidin bound) from intracellular (unbound) VEGFR2. (F) Cells were treated with VEGF, GO, or a combination of both for 15 min, biotinylated immediately after treatments, and evaluated by immunoblot. β₁ Integrin and GAPDH are the cell surface and intracellular controls. (G) Quantification of relative intracellular VEGFR2 abundance after treatment. *n* = 3 sets of cells. (H) Cells were treated with VEGF, GO, or both, biotinylated after a 12-hour recovery, and evaluated by immunoblot. β₁ Integrin and GAPDH are the cell surface and intracellular controls. (I) Quantification of relative cell surface VEGFR2 abundance after recovery. *n* = 3 sets of cells. (J and K) Immunoblot (J) and quantification (K) of total VEGFR2 and pVEGFR2 treated with VEGF 12 hours after recovery from an initial stimulation by VEGF, GO, or a combination of both. *n* = 3 sets of cells. Data represent means ± SEM and were analyzed using a Student's *t* test.

exposure results in a buildup of ROS, which induces ligand- and intrinsic kinase-independent VEGFR2 phosphorylation. In time, this promotes reduction of VEGFR2 in the Golgi compartment, which eventually results in less receptor at the cell surface and decreased angiogenic responses. The findings demonstrate the remarkable versatility of the VEGFR2 signaling system and, in particular, uncover a ligand-independent function of the receptor.

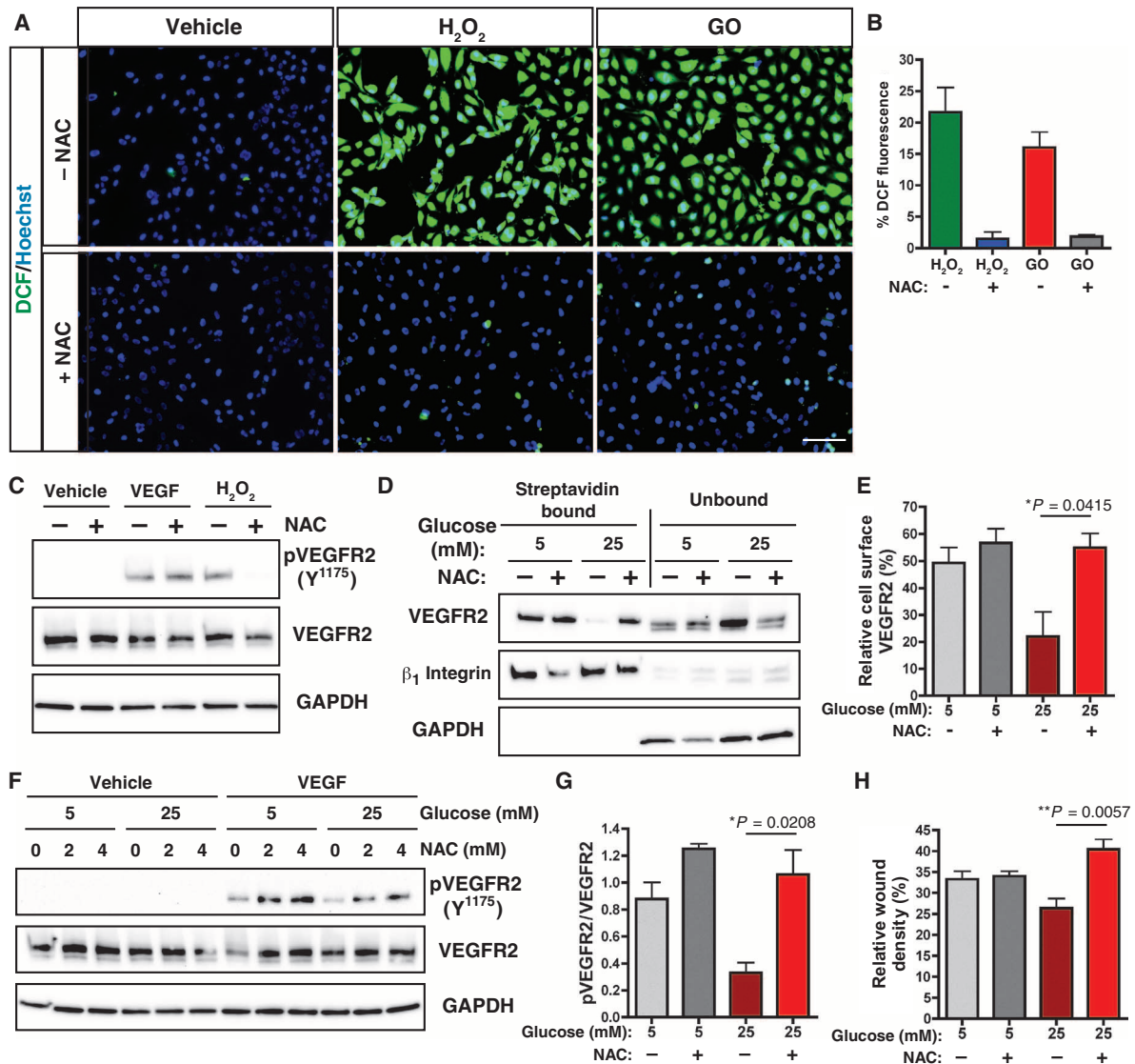


Fig. 6. Antioxidants can rescue the effects of ROS and hyperglycemia on VEGFR2 in endothelial cells. (A) HUVECs treated with H₂O₂ or GO ± NAC were imaged for the ROS indicator DCF (green) and the nuclear stain Hoechst 33342 (blue). Scale bar, 50 μm. (B) Quantification of relative DCF fluorescence. *n* = 12 images from three sets of cells. (C) Immunoblot for total VEGFR2 and pVEGFR2 in HUVECs treated with VEGF or H₂O₂ ± NAC. *n* = 3 sets of cells. (D) Immunoblot of VEGFR2 after cell surface biotinylation of HUVECs cultured in 5 or 25 mM glucose ± NAC. β₁ Integrin and GAPDH

are the membrane and intracellular controls. (E) Quantification of relative cell surface VEGFR2 after cell surface biotinylation. *n* = 3 sets of cells. (F and G) Immunoblot (F) and quantification (G) of total VEGFR2 and pVEGFR2 in HUVECs grown in 5 or 25 mM glucose ± NAC, after stimulation with VEGF. *n* = 3 sets of cells. (H) Wound closure migration assay in HUVECs grown in 5 or 25 mM glucose ± NAC. Relative wound density was plotted 10 hours after wounding. *n* = 3 sets of cells. Data represent means ± SEM and were analyzed using a Student's *t* test.

It has been well documented that the outcome of RTK activation can vary depending on location. Activation of VEGFR2 and epidermal growth factor receptor (EGFR), among others, can occur in distinct areas departing from the plasma membrane, for example, in lipid rafts, caveolae, and endosomes. Compartmentalization of signaling offers spatial control with potentially important consequences for localized activation, as well as control of the extent and duration of the signal (30, 31). In addition, qualitative differences in cell function arise because of recruitment of different sets of effectors that might not be equally represented in distinct parts of the cell.

Activation within the Golgi is unprecedented for VEGFR2, but has been reported for other intracellular signaling molecules such as eNOS (endothelial nitric oxide synthase) and Src (32, 33). Whereas it was previously thought that signaling proteins found in the Golgi were either inactive or immature forms en route to the plasma membrane, increasing evidence supports a role for active signaling from the Golgi that plays distinct functional roles. For example, eNOS can be phosphorylated in the Golgi in endothelial cells in vitro (32) and in vivo (34), and Golgi-localized eNOS is necessary for optimal nitric oxide production. VEGF signaling can activate eNOS both at the cell surface and in the Golgi (32); however,

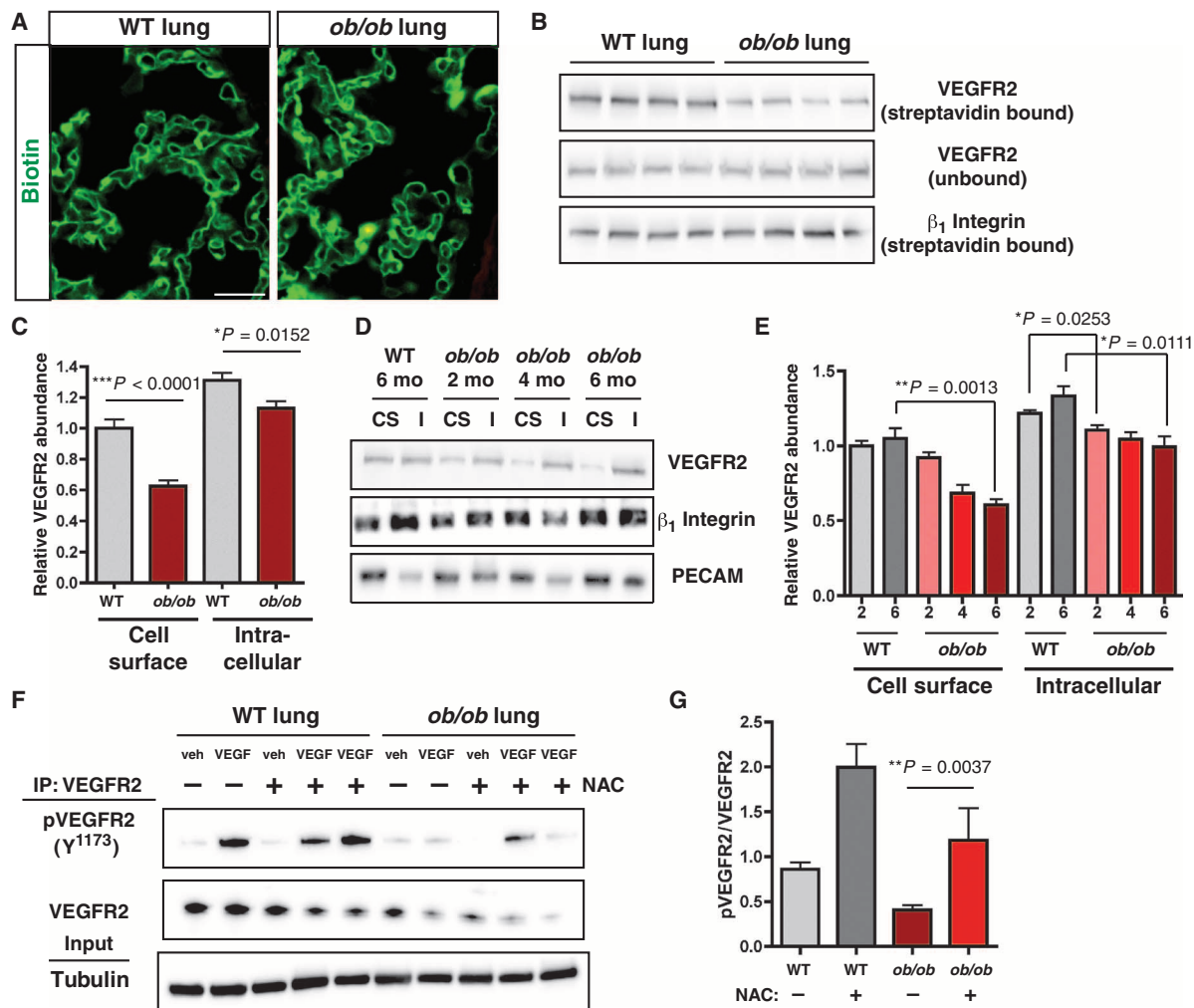


Fig. 7. Antioxidants can rescue the effects of ROS and hyperglycemia on VEGFR2 in diabetic mice. (A) Immunofluorescence of lungs from WT and *ob/ob* mice after perfusion with biotin (green). Scale bar, 25 μ m. $n = 10$ mice. (B) Immunoblot of in vivo cell surface biotinylation to separate cell surface (streptavidin bound) and intracellular (unbound) VEGFR2 in lungs from *ob/ob* and WT mice. β_1 Integrin is a control. (C) Quantification of relative cell surface and intracellular VEGFR2 in lungs from WT and *ob/ob* mice. $n = 10$ mice. (D and E) Lungs from *ob/ob* mice of the

indicated ages evaluated by immunoblot (D) and quantification (E) of cell surface and intracellular abundance of VEGFR2. $n = 4$ mice per condition. β_1 Integrin and PECAM are membrane controls. (F and G) WT and *ob/ob* mice exposed to NAC or vehicle throughout their lifetime were perfused with VEGF or vehicle control. Immunoblots (F) and quantification (G) of total VEGFR2 and pVEGFR2 after immunoprecipitation of VEGFR2. $n = 3$ to 9 mice per condition. Data represent means \pm SEM and were analyzed using a Student's t test.

whether Golgi activation occurs locally has not been explored. The findings presented in this study open this possibility.

Src is another protein that is activated in association with the Golgi compartment, which is of particular importance because our findings implicate this kinase in the phosphorylation of VEGFR2. Activation of Src family kinases at the Golgi can regulate retrograde trafficking (33, 35). Src activation at the Golgi can be induced by growth factor stimulation (36) or oxidative stress (37). The findings reported here show a mode of VEGFR2 signaling that is Src-dependent and occurs under oxidative stress. Similar Src-dependent activation of VEGFR2 has been reported under conditions of fluid shear stress (38) and for VEGFR3 upon endothelial cell adhesion to the extracellular matrix (23) and in sprouting angiogenesis (24). In addition, Src-dependent activation of EGFR under oxidative stress has been reported to occur in a ligand-independent manner and cannot be blocked

by inhibitors against EGFR kinase activity. However, ROS-mediated phosphorylation of EGFR occurs at the cell surface and induces stabilization of the receptor at the plasma membrane (39). Together, these findings (EGFR, VEGFR3, and VEGFR2, in this work) provide an alternate mechanism of signaling by RTKs. In addition to activation through receptor dimerization induced by ligands, the option of ligand-independent phosphorylation through other kinases can also occur, which appears to require Src. However, the downstream consequences of ligand-independent Src-mediated signaling might be distinct for individual RTKs.

Induction of VEGFR2 signaling by ROS has been reported previously, although in a manner requiring VEGF ligation (11, 40–42). Through a mechanism common to other RTKs, VEGF binding to VEGFR2 induces ROS production, which is necessary for activation of downstream signaling. Activation of RTK signaling programs by low concentrations of ROS

likely aids in normal cell function in the short term, but as shown here, long-term ROS exposure results in the exhaustion of these pathways, leading to endothelial damage. In agreement with this concept and our observations, down-regulation of the antioxidant peroxiredoxin II also results in inactivation of VEGF-VEGFR2 signaling (43).

The VEGF-VEGFR2 axis controls various endothelial cell functions ranging from migration to proliferation to survival. Differences in signaling outcomes by the same receptor are dictated by varying the modes of activation. For example, the manner in which VEGF is presented to VEGFR2 directs the formation of functionally and molecularly distinct complexes resulting in distinct modes of vascular expansion (44). Activation of VEGFR2 by soluble VEGF leads to preferential activation of Akt and receptor association with neuropilin 1 and β_3 integrins (45–47). In contrast, activation of VEGFR2 by VEGF that is bound to the extracellular matrix results in receptor binding with β_1 integrins and activation of p38. Furthermore, activation of intracellular VEGFR2 by VEGF produced by endothelial cells promotes endothelial cell survival (22). This work presents an additional layer of versatility in the modes of VEGFR2 signaling, whereby its phosphorylation in the Golgi compartment occurs in a ligand- and intrinsic kinase-independent fashion, offering the option for rapid and perhaps monomeric signaling at a site far from the cell membrane.

MATERIALS AND METHODS

Mice

ob/ob (48) and STZ mice were obtained from The Jackson Laboratory. VE-Cadherin-Cre transgenic mice (49) were crossed to VEGF^{lox/lox} mice (50) to generate VEGF endothelial cell knockout (VEGF^{ECKO}) mice (22). *src*^{-/-} (51) and *fyn*^{-/-} (52) mice were obtained from J. Cooper (Fred Hutchinson Cancer Research Center). Experimental procedures were performed in accordance with university guidelines.

Cells

HUVECs (Vec Technologies) and liver endothelial cells from VEGF^{ECKO} or wild-type mice (22) were cultured in MCDB 131 (Vec Technologies) with 10% fetal bovine serum (FBS). 293 cells (American Type Culture Collection) were cultured in Dulbecco's modified Eagle's medium (DMEM) (Invitrogen) with 10% FBS. Cells were maintained at 37°C with 5% CO₂. Cells cultured under high glucose were grown in the presence of 25 mM glucose for a minimum of 5 days.

Angiogenesis assays

For wound-healing assays, full-thickness, excisional skin wounds were performed under sodium pentobarbital (160 mg/kg) by biopsy punches on the back of the mouse. Wounds were imaged daily with a Nikon Coolpix 995 digital camera. Images were analyzed with ImageJ (National Institutes of Health). For matrix gel assays, mice were injected subcutaneously with collagen type I (3 mg/ml) (BD Biosciences), fibrinogen (1 mg/ml) [with aprotinin (0.1 U/ml) and thrombin (0.5 U/ml)], VEGF (1 μ g/ml), and DMEM. After 7 days, explants were removed and fixed in 2% paraformaldehyde. Confocal images of sections stained for PECAM were processed by ImageJ to generate average Z-projected images. Vascular density was quantified with AngioTool (53).

Tyrosine phosphorylation assays

Cells were starved in serum-free medium overnight. Cells were treated with 200 μ M Na₃VO₄ in MCDB 131 for 5 min at 37°C, then VEGF (100 ng/ml) in MCDB 131 for 5 min, or with GO (1 U/ml) or 500 μ M H₂O₂ in MCDB 131 for 5 to 90 min at 37°C. In experiments using inhibitors, cells were

pretreated with the indicated inhibitor for 2 hours at 37°C. Cells were lysed in modified radioimmunoprecipitation assay (mRIPA) buffer as described previously (47). For in vivo assays, mice were perfused with 10 ml of 200 μ M Na₃VO₄ in serum-free DMEM, then either 10 ml of VEGF (200 ng/ml), 1 mM H₂O₂, or vehicle in serum-free DMEM. Total lungs were lysed in mRIPA (100 μ l mRIPA/10 mg lung), homogenized, and centrifuged to clear debris. The following inhibitors were used at the indicated concentrations: anti-VEGF antibody, 10 μ g/ml (Genentech); SU4312, 20 μ M (Sigma); PP2, 10 μ M (Millipore); NAC, 0.2 to 4 mM for in vitro experiments, 5 mg/ml for mouse experiments (Sigma).

Quantitative real-time PCR

The following primers were used: *Vegfr2*, 5'-GATGAGCGCTGTGAACGCTT-3' (forward) and 5'-CTGCCTCAATCACTTGGCCG-3' (reverse); *Vegfa*, 5'-CAGGCTGCTGTAACGATGAA-3' (forward) and 5'-GCATTACATCTGCTGTGCT-3' (reverse); *Hprt*, 5'-CTGGTTAAGCAGTACAGCCCCAA-3' (forward) and 5'-CGAGAGGTCCTTTTACCAGC-3' (reverse). Each reaction was run in duplicate, normalized, and calculated relative to *Hprt*.

Migration assay

Cells were starved in MCDB 131 + 0.1% FBS overnight. Wounds were created with a 96-pin WoundMaker (Essen). Cells were washed and grown in MCDB 131 + 0.1% FBS with 5 or 25 mM glucose, \pm NAC, \pm VEGF (100 ng/ml). Images were taken every 2 hours with an IncuCyte Imaging System (Essen).

Cell surface biotinylation

HUVECs were washed with Hanks' balanced salt solution (HBSS) and then labeled with sulfo-NHS-SS-biotin (0.5 mg/ml) (Pierce) in HBSS for 30 min at 4°C. The labeling reaction was stopped with MCDB 131. Cells were harvested in mRIPA. Lysates (100 μ g) were incubated with 30 μ l of streptavidin-agarose (Pierce) for 2 hours at 4°C. Unbound supernatant was separated. Bound proteins were washed with mRIPA and eluted with Laemmli buffer. In vivo biotinylation was performed as described previously (54).

Subcellular fractionation

HUVECs (2 \times 100-mm plates per condition) were harvested, and fractionation was done as described previously (32). Fractions (1 ml) were taken from the top of the gradient and concentrated with StrataClean beads (Stratagene).

Ligand-binding assays for Scatchard analysis

VEGF-A (PeproTech) and VEGF-E (ProSpec) were iodinated with the chloramine-T method. Free iodine was less than 2%, and the specific activity was calculated as 172,000 cpm/ng for VEGF-A and 243,000 cpm/ng for VEGF-E. For Scatchard analysis, confluent cultures were exposed to either 5 or 25 mM glucose for 5 days. Cells were washed and incubated with labeled VEGF for 30 min at 4°C in binding buffer [DMEM, 1% bovine serum albumin, 25 mM HEPES (pH 7.4)] with increasing amounts of unlabeled VEGF. Cultures were washed and lysed (0.1% SDS and 0.3 M NaOH). Radioactivity was determined with a gamma counter. Nonspecific binding was determined with 100-fold molar excess of unlabeled growth factor.

DCF assay

HUVECs were exposed to 5 or 25 mM glucose for 5 days. Cells exposed to exogenous ROS were treated with GO (1 U/ml) or 500 μ M H₂O₂ for 15 min, washed in HBSS, and incubated with DCF (Molecular Probes) for 30 min and Hoechst 33342 during the last 5 min. After washing, cells were imaged with Axiovert 200M fluorescence microscope (Zeiss) and analyzed with ImageJ.

Cell surface proteolysis assay

HUVECs were serum-starved overnight and then treated with 0.25% trypsin + 0.02% EDTA in phosphate-buffered saline for 45 s to cleave cell surface proteins. The reaction was stopped with MCDB 131 + 1% FBS. Cells were treated with VEGF or ROS as described above.

Statistical analyses

Computation and examination of normal quantile (percentile) plots for the distribution of continuous data were done to determine that the data follow normal distribution on the original scale. Data were evaluated with unpaired two-tailed Student's *t* tests, where **P* < 0.05, ***P* < 0.01, and ****P* < 0.001. Data are presented as means ± SEM.

SUPPLEMENTARY MATERIALS

www.sciencesignaling.org/cgi/content/full/7/307/ra1/DC1

Fig. S1. Blood glucose concentrations and *Vegfa* and *Vegfr2* transcript abundance in diabetic mice.

Fig. S2. Images of wound closure migration and Scatchard plots for VEGF-A under normal and high-glucose concentrations.

Fig. S3. ROS-mediated activation of VEGFR2 in different endothelial cell types.

Fig. S4. Activation of Src family members.

Fig. S5. Activation of Tie2 and signaling downstream of VEGFR2 by ROS.

Fig. S6. Immunofluorescence of phosphorylated Src within the Golgi compartment.

REFERENCES AND NOTES

- C. C. L. Wang, J. E. B. Reusch, Diabetes and cardiovascular disease: Changing the focus from glycemic control to improving long-term survival. *Am. J. Cardiol.* **110**, 58B–68B (2012).
- A. Martin, M. R. Komada, D. C. Sane, Abnormal angiogenesis in diabetes mellitus. *Med. Res. Rev.* **23**, 117–145 (2003).
- U. Hink, H. Li, H. Mollnau, M. Oelze, E. Matheis, M. Hartmann, M. Skatchkov, F. Thaiss, R. A. Stahl, A. Warnholtz, T. Meinertz, K. Griendling, D. G. Harrison, U. Forstermann, T. Munzel, Mechanisms underlying endothelial dysfunction in diabetes mellitus. *Circ. Res.* **88**, E14–E22 (2001).
- C. Rask-Madsen, G. L. King, Vascular complications of diabetes: Mechanisms of injury and protective factors. *Cell Metab.* **17**, 20–33 (2013).
- F. Giacco, M. Brownlee, Oxidative stress and diabetic complications. *Circ. Res.* **107**, 1058–1070 (2010).
- P. Geraldes, G. L. King, Activation of protein kinase C isoforms and its impact on diabetic complications. *Circ. Res.* **106**, 1319–1331 (2010).
- A. Goldin, J. A. Beckman, A. M. Schmidt, M. A. Creager, Advanced glycation end products: Sparking the development of diabetic vascular injury. *Circulation* **114**, 597–605 (2006).
- T. Nishikawa, D. Edelstein, X. L. Du, S. Yamagishi, T. Matsumura, Y. Kaneda, M. A. Yorek, D. Beebe, P. J. Oates, H. P. Hammes, I. Giardino, M. Brownlee, Normalizing mitochondrial superoxide production blocks three pathways of hyperglycaemic damage. *Nature* **404**, 787–790 (2000).
- M. Sundaresan, Z. X. Yu, V. J. Ferrans, K. Irani, T. Finkel, Requirement for generation of H₂O₂ for platelet-derived growth factor signal transduction. *Science* **270**, 296–299 (1995).
- Y. S. Bae, S. W. Kang, M. S. Seo, I. C. Baines, E. Tekle, P. B. Chock, S. G. Rhee, Epidermal growth factor (EGF)-induced generation of hydrogen peroxide. Role in EGF receptor-mediated tyrosine phosphorylation. *J. Biol. Chem.* **272**, 217–221 (1997).
- M. Ushio-Fukai, Y. Tang, T. Fukui, S. I. Dikalov, Y. Ma, M. Fujimoto, M. T. Quinn, P. J. Pagano, C. Johnson, R. W. Alexander, Novel role of gp91^{phox}-containing NAD(P)H oxidase in vascular endothelial growth factor–induced signaling and angiogenesis. *Circ. Res.* **91**, 1160–1167 (2002).
- N. Ferrara, Vascular endothelial growth factor: Basic science and clinical progress. *Endocr. Rev.* **25**, 581–611 (2004).
- C. M. Warren, M. L. Iruela-Arispe, Signaling circuitry in vascular morphogenesis. *Curr. Opin. Hematol.* **17**, 213–218 (2010).
- P. Carmeliet, V. Ferreira, G. Breier, S. Pollefeyt, L. Kieckens, M. Gertsenstein, M. Fahrig, A. Vandenhoeck, K. Harpal, C. Eberhardt, C. Declercq, J. Pawling, L. Moons, D. Collen, W. Risau, A. Nagy, Abnormal blood vessel development and lethality in embryos lacking a single VEGF allele. *Nature* **380**, 435–439 (1996).
- N. Ferrara, K. Carver-Moore, H. Chen, M. Dowd, L. Lu, K. S. O'Shea, L. Powell-Braxton, K. J. Hillan, M. W. Moore, Heterozygous embryonic lethality induced by targeted inactivation of the VEGF gene. *Nature* **380**, 439–442 (1996).
- F. Shalaby, J. Rossant, T. P. Yamaguchi, M. Gertsenstein, X. F. Wu, M. L. Breitman, A. C. Schuh, Failure of blood-island formation and vasculogenesis in Flk-1-deficient mice. *Nature* **376**, 62–66 (1995).
- R. L. Kendall, R. Z. Rutledge, X. Mao, A. J. Tebben, R. W. Hungate, K. A. Thomas, Vascular endothelial growth factor receptor KDR tyrosine kinase activity is increased by autophosphorylation of two activation loop tyrosine residues. *J. Biol. Chem.* **274**, 6453–6460 (1999).
- E. Chou, I. Suzuma, K. J. Way, D. Opland, A. C. Clermont, K. Naruse, K. Suzuma, N. L. Bowling, C. J. Vlahos, L. P. Aiello, G. L. King, Decreased cardiac expression of vascular endothelial growth factor and its receptors in insulin-resistant and diabetic states: A possible explanation for impaired collateral formation in cardiac tissue. *Circulation* **105**, 373–379 (2002).
- F. C. Sasso, D. Torella, O. Carbonara, G. M. Ellison, M. Torella, M. Scardone, C. Marra, R. Nasti, R. Marfella, D. Cozzolino, C. Indolfi, M. Cotrufo, R. Torella, T. Salvatore, Increased vascular endothelial growth factor expression but impaired vascular endothelial growth factor receptor signaling in the myocardium of type 2 diabetic patients with chronic coronary heart disease. *J. Am. Coll. Cardiol.* **46**, 827–834 (2005).
- P. Lindström, The physiology of obese-hyperglycemic mice [ob/ob mice]. *Scientific World Journal* **7**, 666–685 (2007).
- O. Seitz, C. Schürmann, N. Hermes, E. Müller, J. Pfeilschifter, S. Frank, I. Goren, Wound healing in mice with high-fat diet- or ob gene-induced diabetes-obesity syndromes: A comparative study. *Exp. Diabetes Res.* **2010**, 476969 (2010).
- S. Lee, T. T. Chen, C. L. Barber, M. C. Jordan, J. Murdock, S. Desai, N. Ferrara, A. Nagy, K. P. Roos, M. L. Iruela-Arispe, Autocrine VEGF signaling is required for vascular homeostasis. *Cell* **130**, 691–703 (2007).
- F. Galvagni, S. Pennacchini, A. Salameh, M. Rocchigiani, F. Neri, M. Orlandini, F. Petraglia, S. Gotta, G. L. Sardone, G. Matteucci, G. C. Terstappen, S. Oliviero, Endothelial cell adhesion to the extracellular matrix induces c-Src-dependent VEGFR-3 phosphorylation without the activation of the receptor intrinsic kinase activity. *Circ. Res.* **106**, 1839–1848 (2010).
- T. Tammela, G. Zarkada, H. Nurmi, L. Jakobsson, K. Heinolainen, D. Tvorogov, W. Zheng, C. A. Franco, A. Murtomäki, E. Aranda, N. Miura, S. Ylä-Herttuala, M. Fruttiger, T. Mäkinen, A. Eichmann, J. W. Pollard, H. Gerhardt, K. Alitalo, VEGFR-3 controls tip to stalk conversion at vessel fusion sites by reinforcing Notch signalling. *Nat. Cell Biol.* **13**, 1202–1213 (2011).
- S. Koch, S. Tugues, X. Li, L. Gualandi, L. Claesson-Welsh, Signal transduction by vascular endothelial growth factor receptors. *Biochem. J.* **437**, 169–183 (2011).
- A. Tiwari, J. J. Jung, S. M. Inamdar, D. Nihalani, A. Choudhury, The myosin motor Myo1c is required for VEGFR2 delivery to the cell surface and for angiogenic signaling. *Am. J. Physiol. Heart Circ. Physiol.* **304**, H687–H696 (2013).
- M. G. Lampugnani, F. Orsenigo, M. C. Gagliani, C. Tacchetti, E. Dejana, Vascular endothelial cadherin controls VEGFR-2 internalization and signaling from intracellular compartments. *J. Cell Biol.* **174**, 593–604 (2006).
- V. Manickam, A. Tiwari, J. J. Jung, R. Bhattacharya, A. Goel, D. Mukhopadhyay, A. Choudhury, Regulation of vascular endothelial growth factor receptor 2 trafficking and angiogenesis by Golgi localized t-SNARE syntaxin 6. *Blood* **117**, 1425–1435 (2011).
- Y. Okuno, A. Nakamura-Ishizu, K. Otsu, T. Suda, Y. Kubota, Pathological neoangiogenesis depends on oxidative stress regulation by ATM. *Nat. Med.* **18**, 1208–1216 (2012).
- A. Disanza, E. Frittoli, A. Palamidessi, G. Scita, Endocytosis and spatial restriction of cell signaling. *Mol. Oncol.* **3**, 280–296 (2009).
- A. A. Lanahan, K. Hermans, F. Claes, J. S. Kerley-Hamilton, Z. W. Zhuang, F. J. Giordano, P. Cameli, M. Simons, VEGF receptor 2 endocytic trafficking regulates arterial morphogenesis. *Dev. Cell* **18**, 713–724 (2010).
- D. Fulton, J. Fontana, G. Sowa, J. P. Gratton, M. Lin, K. X. Li, B. Michell, B. E. Kemp, D. Rodman, W. C. Sessa, Localization of endothelial nitric-oxide synthase phosphorylated on serine 1179 and nitric oxide in Golgi and plasma membrane defines the existence of two pools of active enzyme. *J. Biol. Chem.* **277**, 4277–4284 (2002).
- F. Bard, L. Mazelin, C. Péchoux-Longin, V. Malhotra, P. Jurdic, Src regulates Golgi structure and KDEL receptor-dependent retrograde transport to the endoplasmic reticulum. *J. Biol. Chem.* **278**, 46601–46606 (2003).
- R. van Haperen, C. Cheng, B. M. E. Mees, E. van Deel, M. de Waard, L. C. A. van Damme, T. van Gent, T. van Aken, R. Krams, D. J. Duncker, R. de Crom, Functional expression of endothelial nitric oxide synthase fused to green fluorescent protein in transgenic mice. *Am. J. Pathol.* **163**, 1677–1686 (2003).
- M. Hiyoshi, N. Takahashi-Makise, Y. Yoshidomi, N. Chutiwitoonchai, T. Chihara, M. Okada, N. Nakamura, S. Okada, S. Suzu, HIV-1 Nef perturbs the function, structure, and signaling of the Golgi through the Src kinase Hck. *J. Cell. Physiol.* **227**, 1090–1097 (2012).
- D. J. Gill, J. Chia, J. Senewiratne, F. Bard, Regulation of O-glycosylation through Golgi-to-ER relocation of initiation enzymes. *J. Cell Biol.* **189**, 843–858 (2010).
- D. Matsuda, Y. Nakayama, S. Horimoto, T. Kuga, K. Ikeda, K. Kasahara, N. Yamaguchi, Involvement of Golgi-associated Lyn tyrosine kinase in the translocation of annexin II to the endoplasmic reticulum under oxidative stress. *Exp. Cell Res.* **312**, 1205–1217 (2006).
- Z. G. Jin, H. Ueba, T. Tanimoto, A. O. Lungu, M. D. Frame, B. C. Berk, Ligand-independent activation of vascular endothelial growth factor receptor 2 by fluid shear stress regulates activation of endothelial nitric oxide synthase. *Circ. Res.* **93**, 354–363 (2003).

39. S. Filosto, E. M. Khan, E. Tognon, C. Becker, M. Ashfaq, T. Ravid, T. Goldkorn, EGF receptor exposed to oxidative stress acquires abnormal phosphorylation and aberrant activated conformation that impairs canonical dimerization. *PLoS One* **6**, e23240 (2011).
40. S. Ikeda, M. Ushio-Fukai, L. Zuo, T. Tojo, S. Dikalov, N. A. Patrushev, R. W. Alexander, Novel role of ARF6 in vascular endothelial growth factor-induced signaling and angiogenesis. *Circ. Res.* **96**, 467–475 (2005).
41. J. Oshikawa, N. Urao, H. W. Kim, N. Kaplan, M. Razvi, R. McKinney, L. B. Poole, T. Fukai, M. Ushio-Fukai, Extracellular SOD-derived H₂O₂ promotes VEGF signaling in caveolae/lipid rafts and post-ischemic angiogenesis in mice. *PLoS One* **5**, e10189 (2010).
42. M. Lee, W. C. Choy, M. R. Abid, Direct sensing of endothelial oxidants by vascular endothelial growth factor receptor-2 and c-Src. *PLoS One* **6**, e28454 (2011).
43. D. H. Kang, D. J. Lee, K. W. Lee, Y. S. Park, J. Y. Lee, S. H. Lee, Y. J. Koh, G. Y. Koh, C. Choi, D. Y. Yu, J. Kim, S. W. Kang, Peroxiredoxin II is an essential antioxidant enzyme that prevents the oxidative inactivation of VEGF receptor-2 in vascular endothelial cells. *Mol. Cell* **44**, 545–558 (2011).
44. S. Lee, S. M. Jilani, G. V. Nikolova, D. Carpizo, M. L. Iruela-Arispe, Processing of VEGF-A by matrix metalloproteinases regulates bioavailability and vascular patterning in tumors. *J. Cell Biol.* **169**, 681–691 (2005).
45. H. Kawamura, X. Li, K. Goishi, L. A. van Meeteren, L. Jakobsson, S. Cébe-Suarez, A. Shimizu, D. Edholm, K. Ballmer-Hofer, L. Kjellén, M. Klagsbrun, L. Claesson-Welsh, Neuropilin-1 in regulation of VEGF-induced activation of p38MAPK and endothelial cell organization. *Blood* **112**, 3638–3649 (2008).
46. S. D. Robinson, L. E. Reynolds, V. Kostourou, A. R. Reynolds, R. G. da Silva, B. Tavora, M. Baker, J. F. Marshall, K. M. Hodivala-Dilke, $\alpha\beta 3$ Integrin limits the contribution of neuropilin-1 to vascular endothelial growth factor-induced angiogenesis. *J. Biol. Chem.* **284**, 33966–33981 (2009).
47. T. T. Chen, A. Luque, S. Lee, S. M. Anderson, T. Segura, M. L. Iruela-Arispe, Anchorage of VEGF to the extracellular matrix conveys differential signaling responses to endothelial cells. *J. Cell Biol.* **188**, 595–609 (2010).
48. Y. Zhang, R. Proenca, M. Maffei, M. Barone, L. Leopold, J. M. Friedman, Positional cloning of the mouse obese gene and its human homologue. *Nature* **372**, 425–432 (1994).
49. J. A. Alva, A. C. Zovein, A. Monvoisin, T. Murphy, A. Salazar, N. L. Harvey, P. Carmeliet, M. L. Iruela-Arispe, VE-Cadherin-Cre-recombinase transgenic mouse: A tool for lineage analysis and gene deletion in endothelial cells. *Dev. Dyn.* **235**, 759–767 (2006).
50. H. P. Gerber, K. J. Hillan, A. M. Ryan, J. Kowalski, G. A. Keller, L. Rangell, B. D. Wright, F. Radtke, M. Aguet, N. Ferrara, VEGF is required for growth and survival in neonatal mice. *Development* **126**, 1149–1159 (1999).
51. P. Soriano, C. Montgomery, R. Geske, A. Bradley, Targeted disruption of the c-src proto-oncogene leads to osteopetrosis in mice. *Cell* **64**, 693–702 (1991).
52. M. W. Appleby, J. A. Gross, M. P. Cooke, S. D. Levin, X. Qian, R. M. Perlmutter, Defective T cell receptor signaling in mice lacking the thymic isoform of p59^{lck}. *Cell* **70**, 751–763 (1992).
53. E. Zudaire, L. Gambardella, C. Kurcz, S. Vermeren, C. Ruhrberg, A computational tool for quantitative analysis of vascular networks. *PLoS One* **6**, e27385 (2011).
54. J. N. Rybak, A. Ettore, B. Kaissling, R. Giavazzi, D. Neri, G. Elia, In vivo protein biotinylation for identification of organ-specific antigens accessible from the vasculature. *Nat. Methods* **2**, 291–298 (2005).

Acknowledgments: We thank M. Steel for animal assistance, S. Memarsadeghi and J. Mack for assistance with InCuCyte experiments, and the Tissue Procurement Core Laboratory.

Funding: This study was supported by NIH National Heart, Lung, and Blood Institute grant RO1CA126935 to M.L.I.-A. and Ruth L. Kirschstein National Research Service Award T32HL69766 to C.M.W. **Author contributions:** C.M.W., S.Z., A.B., A.D., and M.L.I.-A. performed the experiments. C.M.W. and M.L.I.-A. designed the experiments and wrote the manuscript. **Competing interests:** The authors declare that they have no competing interests.

Submitted 10 April 2013
Accepted 6 December 2013
Final Publication 7 January 2014
10.1126/scisignal.2004235

Citation: C. M. Warren, S. Ziyad, A. Briot, A. Der, M. L. Iruela-Arispe, A ligand-independent VEGFR2 signaling pathway limits angiogenic responses in diabetes. *Sci. Signal.* **7**, ra1 (2014).